Applied Magnetic Resonance (2022) 53:797–808
https://doi.org/10.1007/s00723-021-01405-3

Applied
Magnetic Resonance

ORIGINAL PAPER

Impact of Chlorine Substitution on Electron Spin Relaxation of a Trityl Radical

Whylder Moore[1] · Justin L. Huffman[2] · Benoit Driesschaert[2] · Sandra S. Eaton[1] · Gareth R. Eaton[1]

Received: 3 May 2021 / Revised: 23 July 2021 / Accepted: 30 July 2021 /
Published online: 12 August 2021

Abstract

A perchlorotriarylmethyl tricarboxylic acid radical 99% enriched in ^{13}C at the central carbon ($^{13}C_1$-PTMTC) was characterized in phosphate-buffered saline solution (pH = 7.2) (PBS) at ambient temperature. Samples immobilized in 1:1 PBS:glycerol or in 9:1 trehalose:sucrose were studied as a function of temperature. Isotope enrichment at C_1 creates a trityl that can be used to accurately measure microscopic viscosity. Understanding of the impact of the ^{13}C hyperfine interaction on electron spin relaxation is important for application of this trityl in oximetry and distance measurements. The anisotropic $^{13}C_1$ hyperfine couplings ($A_x = A_y = 24 \pm 2$ MHz, $A_z = 200 \pm 1$ MHz) are larger than for the related $^{13}C_1$-perdeuterated Finland trityl ($^{13}C_1$-dFT) and the g anisotropy ($g_x = 2.0013$, $g_y = 2.0016$, $g_z = 2.0042$) is slightly larger than for $^{13}C_1$-dFT. The tumbling correlation times (τ_R) for $^{13}C_1$-PTMTC are 0.20 ± 0.02 ns in PBS and 0.40 ± 0.05 ns in 3:1 PBS:glycerol, which are shorter than for $^{13}C_1$-dFT in the same solutions. T_1 for $^{13}C_1$-PTMTC is 3.5 ± 0.5 µs in PBS and 5.3 ± 0.4 µs in 3:1 PBS:glycerol, which are shorter than for $^{13}C_1$-dFT due to faster tumbling, larger anisotropy of the $^{13}C_1$ hyperfine, and about 30% larger contribution from the local mode. In immobilized samples, T_1 for $^{13}C_1$-PTMTC is similar to that for $^{13}C_1$-dFT and other trityls without chlorine or $^{13}C_1$ substituents, indicating that the $^{13}C_1$ and Cl substituents on the phenyl rings have little impact on T_1. The temperature dependence of T_1 was modeled with contributions from the direct, Raman, and local mode processes. Broadening of CW linewidths of about 0.6 G in fluid solution and about 2 G in rigid lattice is attributed to unresolved $^{35,37}Cl$ hyperfine couplings.

✉ Gareth R. Eaton
Gareth.eaton@du.edu

[1] Department of Chemistry and Biochemistry, University of Denver, Denver, CO 80210, USA

[2] Department of Pharmaceutical Sciences, School of Pharmacy, In Vivo Multifunctional Magnetic Resonance Center, West Virginia University, Morgantown, WV 26506, USA

1 Introduction

Triarylmethyl radicals (TAMs, trityls) have many applications for in vivo oximetry [1–7] and spin labeling [8–13], and are inherently interesting because of their stability and their long electron spin relaxation times. These radicals are carefully designed elaborations of the Gomberg triphenylmethyl radical that was characterized more than a century ago [14]. A wide range of substituents on the aromatic rings affect the EPR hyperfine structure, relaxation times, solubility, aggregation, and reactivity. Major emphasis has been on the class of trityls designed to place atoms with nuclear spins as far as is feasible from the locations of high unpaired spin density to achieve narrow lines. An example is deuterated Finland trityl (dFT) and related species [15]. In parallel, analogous stable radicals in which the phenyl ring substituents include chlorine have been studied extensively by Ballester and coworkers [16]. Understanding of the impact of ring substituents on the electron spin relaxation times is important for the applications of these trityls in oximetry and distance measurements. Initial relaxation studies showed that T_1 for trityls was not strongly influenced by Cl on the phenyl rings [17], although differences in solubility of dFT and PTM required use of different solvents, which made it difficult to distinguish solvent effects from the effects of substituents. We previously compared T_1 in fluid solution for $^{13}C_1$-dFT with that for dFT, which demonstrated the contribution to T_1 from modulation of the ^{13}C hyperfine anisotropy [18]. In this paper, we present T_1 for $^{13}C_1$-PTMTC in fluid solution and T_1 in rigid lattice for $^{13}C_1$-PTMTC and $^{13}C_1$-dFT.

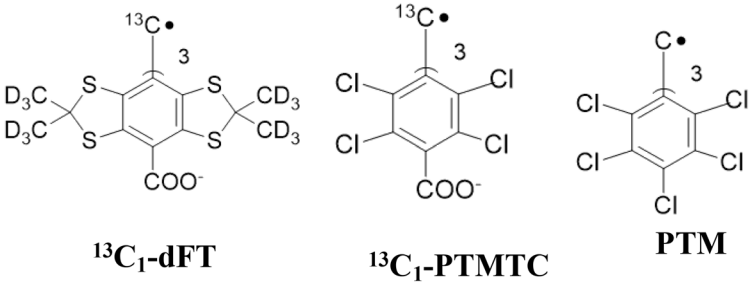

$^{13}C_1$-dFT **$^{13}C_1$-PTMTC** **PTM**

2 Methods

2.1 EPR Sample Preparation

The syntheses of tris(4-carboxy-2,3,5,6-tetrachlorophenyl)methyl radical-$^{13}C_1$ ($^{13}C_1$-PTMTC) and $^{13}C_1$-dFT were performed at West Virginia University as reported in [19] and [20]. Solutions were prepared in 50 mM sodium phosphate buffer containing 142 mM NaCl (PBS), pH = 7.2 with trityl concentrations of 0.5 or 1.0 mM and stored at 4 °C. Samples of $^{13}C_1$-PTMTC were protected from light. Samples for fluid solution spectroscopy at ambient temperature (~20 °C) were contained in Zeus AWG19 thin wall Teflon tubing with an internal diameter of about 0.97 mm

and about 0.1 mm wall thickness. Deoxygenation of the samples was performed with N_2 purging as previously reported [18]. A sample of $^{13}C_1$-PTMTC in 9:1 trehalose:sucrose with a 2000:1 sugar to radical ratio was prepared using the same procedure as for $^{13}C_1$-dFT [18]. Based on a density of trehalose of 1.6 g/mL, the estimated concentrations in the glasses are 2 and 4 mM for $^{13}C_1$-dFT and $^{13}C_1$-PTMTC, respectively. Samples in 1:1 PBS:glycerol or in 9:1 trehalose:sucrose glass were in 4 mm OD quartz tubes for X-band or 1.6 mM OD capillaries for Q-band. Relaxation time measurements were performed on immobilized samples that had been deoxygenated by freeze–pump–thaw degassing and back-filling with a partial pressure of helium to provide thermal conductivity.

2.2 EPR Spectra

Fluid solution spectra were recorded on a Bruker EMX at X-band with an SHQE resonator and on a Bruker E580 at Q-band. Spectra were acquired with non-saturating microwave power and modulation frequency of 100 kHz. The modulation amplitude was 0.2 G for samples in PBS at X-band, 0.3 G for 3:1 PBS:glycerol at X-band and 0.6 G for PBS at Q-band. Pulsed EPR measurements were made using a Bruker E580 with an X-band dielectric resonator in a CF935 flow cryostat cooled by liquid N_2 boiloff gas or by He gas, cooled with a Bruker/ColdEdge Stinger closed cycle system. CW spectra at 160 K were acquired at 60 dB attenuation ($B_1 \sim 0.9$ mG) to minimize power saturation and passage effects. T_1 was measured by 3-pulse inversion recovery, with pulse lengths from ca. 40 to 120 ns. For each pulse length, the output of a 1 kW TWT was attenuated to yield the maximum echo amplitude. Above the glass transition temperature, incomplete motional averaging of the A anisotropy makes T_m for $^{13}C_1$-dFT or $^{13}C_1$-PTMTC too short to detect an echo between ~ 160 and ~ 293 K, so inversion recovery measurements of T_1 in 1:1 PBS:glycerol were performed only up to about 160 K. The rigidity of the 9:1 trehalose:sucrose glasses permits measurements up to room temperature.

2.3 Data Analysis

For immobilized samples, CW spectra and first derivatives of the field-swept echo-detected spectra were simulated using the 'pepper' function of EasySpin [21], and the resulting parameters are shown in Table 1. Parameters obtained from the immobilized spectra were used to simulate the fluid solution spectra with EasySpin and thereby determine the tumbling correlation time, τ_R. The 'garlic' function in EasySpin was used for spectra in PBS, and 'chili' for spectra in 3:1 PBS:glycerol. An approximate value of $T_2 = 110$ ns in fluid solution was calculated using the expression $T_2 = 2/(\sqrt{3}\gamma\Delta B_{pp})$, where γ is the gyromagnetic ratio and $\Delta B_{pp} = 0.6$ G is the tumbling-independent contribution to the peak-to-peak linewidths. The inversion recovery data were fit to the sum of two exponentials and the longer component was attributed to T_1. The dependence of T_1 on tumbling correlation time in fluid solution was modeled as described in [18]. The temperature dependence of T_1 in immobilized samples was modeled as the sum of the direct, Raman, and local mode processes as

Table 1 g[a] and A (MHz) values for trityl radicals

Radical	Solvent	g_x	g_y	g_z	g_{iso}	A_x	A_y	A_z	A_{iso}	Ref
$^{13}C_1$-PTMTC	1:1 PBS:glycerol	2.0013	2.0016	2.0042	2.0024	24	24	200	82.7	This work
$^{13}C_1$-PTMTC	9:1 Trehalose: sucrose	2.0015	2.0015	2.0040	2.0024	26	25	199.5		[19]
PTMTC	1:1 water:glycerol	2.00338	2.00074	2.0002	2.0014					[39]
$^{13}C_1$-PTMTC	DMSO				2.0028				83.5	[23]
PTMTC	Buffer	2.0009	2.0009	2.004						[40]
PTM	Solid				2.0030				81.9	[41]
PTM	CCl_4				2.0026				82.5	[16]
$^{13}C_1$-dFT	9:1 Trehalose:sucrose	2.0033	2.0032	2.00275	2.0031	18	18	162		[18]
dFT	1:1 Water:glycerol	2.0030	2.0027	2.0021	2.0026					[34]

[a]Although the differences in g values can be defined with uncertainties of about ± 0.0002 in the simulations, absolute g values have uncertainties of about ± 0.0004 due to the linewidths for radicals used in the magnetic field calibrations

described previously [17, 22]. The process that is denoted as the direct process may be impacted by cross relaxation between neighboring paramagnetic centers.

3 Results and Discussion

3.1 CW Spectra

X-band and Q-band fluid solution spectra of $^{13}C_1$-PTMTC in deoxygenated solutions at ambient temperature are shown in Fig. 1. The well-resolved $^{13}C_1$ hyperfine of 82.8 MHz = 29.6 G is similar to the values of 83.5 MHz reported for $^{13}C_1$-PTMTC in water [18] and in DMSO [23] and 82.5 MHz for PTM in CCl_4 [16]. The very small sharp peak in the center of the spectrum is due to residual $^{12}C_1$-PTMTC. In deoxygenated samples of $^{13}C_1$-PTMTC in PBS the peak-to-peak linewidths at X-band are 0.96 and 0.90 G for the low-field and high-field lines, respectively. The X-band linewidths in PBS are about 0.15 G narrower than reported in water [19], which is attributed to the use of lower modulation amplitude. Incomplete motional averaging of the g and A anisotropy contributes to the unequal amplitudes (and widths) of the two ^{13}C hyperfine lines and the broader lines for $^{13}C_1$-PTMTC than for $^{12}C_1$-PTMTC. The spectra were simulated with EasySpin using the anisotropic g and A values shown in Table 1 to obtain tumbling correlation times, $\tau_R = 0.20 \pm 0.02$ ns in PBS and 0.40 ± 0.05 ns in 3:1 PBS:glycerol. The much lower intensity satellite

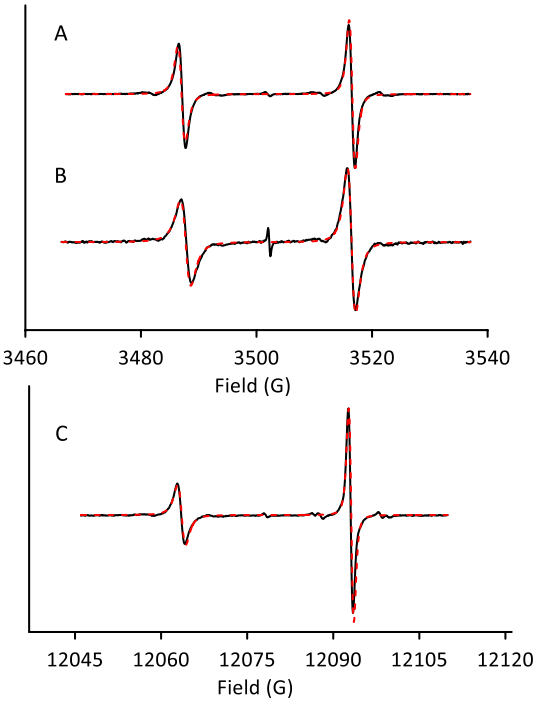

Fig. 1 Room temperature (~20 °C) spectra (black) for deoxygenated solutions of **A** 0.5 mM $^{13}C_1$-PTMTC in 50 mM PBS pH ~ 7.2, **B** 0.5 mM $^{13}C_1$-PTMTC in 3:1 PBS:glycerol (X-band, 9.8151 GHz) and **C** 1.0 mM $^{13}C_1$-PTMTC in PBS (Q-band, 33.8 GHz). Spectra were simulated (red) with EasySpin using $g_x = 2.0013$, $g_y = 2.0016$, $g_z = 2.0042$, $A_x = A_y = 24$, $A_z = 200.5$ MHz for $^{13}C_1$, and $\tau = 0.20$ ns or 0.40 ns for PBS and 3:1 PBS:glycerol, respectively. ΔB_{pp} for Gaussian and Lorentzian contributions to the simulations are 0.62 and 0.15 (G), respectively

lines with hyperfine splittings of about 36 and 29 MHz have been assigned to isotopologues with a ^{13}C at positions C_2 or $C_{3,3'}$, respectively [19]. These contributions were not included in the simulations in Fig. 1. The EasySpin simulations of the fluid solution linewidths include a tumbling-independent Gaussian contribution that was 0.62 G for $^{13}C_1$-PTMTC and 0.06 G for $^{13}C_1$-dFT [18]. The large Gaussian contribution for $^{13}C_1$-PTMTC is attributed to unresolved $^{35,37}Cl$ hyperfine coupling. EasySpin simulations indicate that a linewidth of about 0.6 G could arise from coupling to a set of six Cl with A_{Cl} of ~ 0.24 MHz and a second set of six Cl with A_{Cl} of ~ 0.16 MHz. These hyperfine couplings are in reasonable agreement with values of 0.17 and 0.09 MHz predicted by DFT calculations for PTMTC [24].

The X-band spectrum of $^{13}C_1$-PTMTC in glassy 1:1 PBS:glycerol (Fig. 2) has well-resolved features for the $^{13}C_1$ hyperfine couplings with $A_z = 200 \pm 1$ MHz and $A_x \sim A_y = 24 \pm 2$ MHz, which are larger than for $^{13}C_1$-dFT, consistent with the literature (Table 1). The $A_{||}$ lines are well resolved in the rigid lattice X-band spectra of both $^{13}C_1$-PTMTC and $^{13}C_1$-dFT (Fig. 2), which permits more precise definition of g anisotropy than can be obtained in spectra of samples with natural isotope

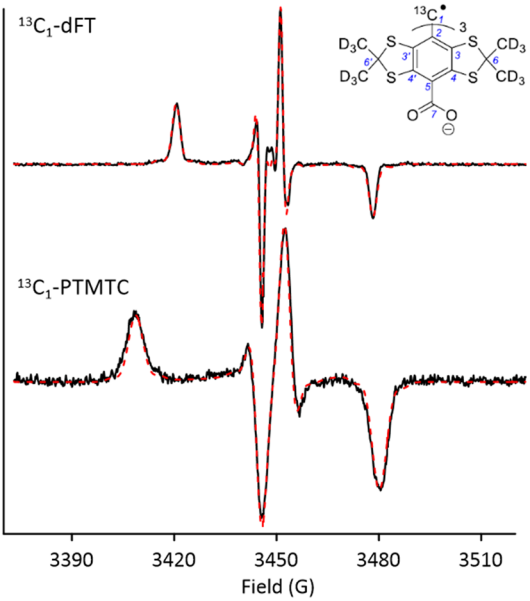

Fig. 2 X-band (9.66 GHz) spectra at ~ 150 K (black) of $^{13}C_1$-dFT and $^{13}C_1$-PTMTC in glassy 3:1 PBS:glycerol acquired with 60 dB attenuation ($B_1 \sim 0.9$ mG) and 1.0 G modulation amplitude at 10 kHz. Spectra were simulated (red) with EasySpin using 'pepper' and the g and A parameters for $^{13}C_1$ listed in Table 1 plus H_{strain} along the x, y, and z axes of 5, 16, and 7.5 MHz for $^{13}C_1$-dFT and 80% of total intensity or H_{strain} along the x, y, and z axes of 10.5, 12, and 14 MHz for $^{13}C_1$-PTMTC with 91% of total intensity, respectively. For $^{13}C_1$-dFT, the isotopologues with a second ^{13}C had coupling constants for $C_{2,3,3'}$ of $A_x = A_y = 30$, $A_z = 36$ MHz with 10% of total intensity and coupling constants for $C_{4,4',5}$ of $A_x = A_y = 14$, $A_z = 13$ MHz with 10% of total intensity. For $^{13}C_1$-PTMTC, the isotopologues with a second ^{13}C had coupling constants for $C_{3,3'}$ of $A_x = A_y = 26$, $A_z = 37$ MHz with 6% of total intensity and coupling constants for C_2 of $A_x = A_y = 33$, $A_z = 41$ MHz with 3% of total intensity

abundance. For $^{13}C_1$-PTMTC the g values are approximately axial with $g_x \sim g_y < g_z$ which is the reverse of $g_x \sim g_y > g_z$ for dFT and $^{13}C_1$-dFT. Small contributions from isotopologues with a second ^{13}C are not well resolved, but were included in the simulations, with the parameters listed in the figure caption. The average values were constrained to match the isotropic couplings observed in fluid solution. The values of the line-broadening parameter H_{strain} that were found in the EasySpin simulations along the parallel axis were 14 MHz for $^{13}C_1$-PTMTC and 7.5 MHz for $^{13}C_1$-dFT. The additional broadening of ~ 6.5 MHz (~ 2 G) is attributed to unresolved chlorine hyperfine. The small anisotropy in g and $A_\perp$ causes uncertainty in linewidths in the perpendicular region of the spectra, so it is difficult to determine the broadening from unresolved chlorine hyperfine in the perpendicular plane.

In PBS, the τ_R for $^{13}C_1$-PTMTC is 0.20 ± 0.02 ns. The molecular radius is calculated to be 6.5 Å [19]. Use of the Stokes–Einstein equation $\tau_R = V\eta/kT$, where V = molecular volume in m^3, η = viscosity in poise, k = Boltzmann's constant = 1.381×10^{-23} J/K, and T = temperature in Kelvin [25] predicts $\tau_R = 0.28$ ns. For relatively small solutes, the Stokes–Einstein model has been modified by inclusion of a slip coefficient, c_{slip}, and becomes $\tau_R = c_{slip} V\eta/kT$ [26, 27]. The ratio 0.20/0.28 gives $c_{slip} = 0.71$ for $^{13}C_1$-PTMTC in PBS, which is intermediate between the $c_{slip} = 0.78$ for $^{13}C_1$-PTMTC in water [19] and $c_{slip} = 0.66$ for dFT in water [18, 28]. The smaller molecular radius for $^{13}C_1$-PTMTC than for dFT (7.5 Å) [28] is consistent with shorter values of τ_R for $^{13}C_1$-PTMTC. In PBS, τ_R for $^{13}C_1$-PTMTC and $^{13}C_1$-dFT is 0.20 ± 0.02 and 0.29 ± 0.02 ns [18], respectively. In 3:1 PBS:glycerol, τ_R for $^{13}C_1$-PTMTC and $^{13}C_1$-dFT is 0.40 ± 0.05 and 0.80 ± 0.05 ns [18], respectively.

3.2 Electron Spin Relaxation Times

The T_2 for $^{13}C_1$-PTMTC in PBS at 293 K measured by 2-pulse spin echo is 110 ± 20 ns which is consistent with the value of 110 ns estimated from the approximately 0.6 G tumbling-independent contribution to the CW lineshapes. The T_1 is 3.5 ± 0.5 µs in PBS and 5.8 ± 0.8 µs in 3:1 PBS:glycerol. The dependence of T_1 on tumbling correlation time in fluid solution was modeled, as reported previously [18], using Eq. (1) which is the sum of contributions from modulation of ^{13}C hyperfine anisotropy $\frac{1}{T_1^A}$(Eq. 2), a local mode $\frac{1}{T_1^{local}}$, spin rotation $\frac{1}{T_1^{SR}}$ (Eq. 3), and modulation of g anisotropy $\frac{1}{T_1^g}$ (Eq. 4) [28–31].

$$\frac{1}{T_1} = \frac{1}{T_1^A} + \frac{1}{T_1^{\text{local}}} + \frac{1}{T_1^{\text{SR}}} + \frac{1}{T_1^g}, \tag{1}$$

$$\frac{1}{T_1^A} = \frac{2}{9} I(I+1) \sum_i (A_i - A_{\text{iso}})^2 \frac{\tau_R}{1 + (\omega\tau_R)^2}, \tag{2}$$

where $I = 1/2$ for ^{13}C, A_i is a component of the ^{13}C nuclear hyperfine in angular frequency units, A_{iso} is the average ^{13}C hyperfine observed in fluid solution, and ω is the Zeeman frequency in angular units.

$$\frac{1}{T_1^{SR}} = \frac{\sum_{i=1}^{3}(g_i - g_e)^2}{9\tau_R}, \tag{3}$$

$$\frac{1}{T_1^{g}} = \frac{2}{5}\left(\frac{\omega}{g}\right)^2\left(\frac{(\Delta g)^2}{3} + (\delta g)^2\right)\frac{\tau_R}{1+(\omega\tau_R)^2}, \tag{4}$$

where $\Delta g = g_{zz} - 0.5(g_{xx}+g_{yy})$, $\delta g = 0.5(g_{xx} - g_{yy})$.

The value of $\frac{1}{T_1^{local}} = 6.6\times10^4\ s^{-1}$ at room temperature was determined previously for natural abundance $^{12}C_1$-dFT and closely related trityls including OX63 [28] in water solution and $7.6\times10^4\ s^{-1}$ for $^{13}C_1$-dFT in PBS [18]. The fit to the experimental values of T_1 in fluid solution (Table 2) was improved by increasing $\frac{1}{T_1^{local}}$ to $(1.0\pm0.2)\times10^5\ s^{-1}$. It is plausible that the chlorine substituents on the trityl rings could impact this parameter.

In the immobilized samples, the echo envelope modulation (ESEEM) from the chlorines was sufficiently deep that it precluded accurate measurements of T_m, so the focus of the relaxation measurements was on T_1. The inversion recovery curves were fit with the sum of two exponentials and the longer time constant was attributed to T_1 [32]. The T_1 obtained by inversion recovery for $^{13}C_1$-PTMTC and $^{13}C_1$-dFT in 1:1 PBS:glycerol and in 9:1 trehalose:sucrose as a function of temperature are plotted in Fig. 3 along with T_1 obtained by inversion recovery for $^{12}C_1$-dFT, $^{12}C_1$-FT in 1:1 water:glycerol, and T_1 obtained by saturation recovery for $^{12}C_1$-dFT and $^{12}C_1$-FT in 1:1 water:glycerol [33, 34]. At the lowest temperatures, T_1 for $^{13}C_1$-PTMTC in 9:1 trehalose:sucrose is shorter than for other samples which is attributed to a larger contribution from the direct process. The estimated concentration in the glass (~4 mM) is higher than for other samples. The large difference in T_1 for $^{13}C_1$-PTMTC between the 9:1 trehalose:sucrose glass and 1:1 PBS:glycerol suggest that there may also be a nonuniform distribution of radicals in the sugar glass. The temperature dependence

Table 2 Contributions to calculated T_1 for $^{13}C_1$-PTMTC in deoxygenated fluid solution[a]

	Calculated with $\tau_R = 0.2\pm0.02$ ns (PBS)	Calculated with $\tau_R = 0.4\pm0.05$ ns (3:1 PBS:glycerol)
$\frac{1}{T_1^A}(s^{-1})$	$(1.77\pm0.14)\times10^5$	$(9.0\pm0.92)\times10^4$
$\frac{1}{T_1^{local}}(s^{-1})$[b]	$(1.0\pm0.2)\times10^5$	$(1.0\pm0.2)\times10^5$
$\frac{1}{T_1^{SR}}(s^{-1})$	$(2.85\pm0.23)\times10^3$	$(1.43\pm0.15)\times10^3$
$\frac{1}{T_1^{g}}(s^{-1})$	$(1.27\pm0.1)\times10^3$	$(6.39\pm0.66)\times10^2$
Calc.$\frac{1}{T_1}(s^{-1})$	$(2.87\pm0.15)\times10^5$	$(2.0\pm0.094)\times10^5$
Calc T_1 (s)	$(3.5\pm0.2)\times10^{-6}$	$(5.1\pm0.3)\times10^{-6}$
Exper. T_1 (s)	$(3.5\pm0.5)\times10^{-6}$	$(5.3\pm0.4)\times10^{-6}$

[a]Calculated using Eqs. (1)–(4)

[b]Adjusted to fit the experimental values of T_1

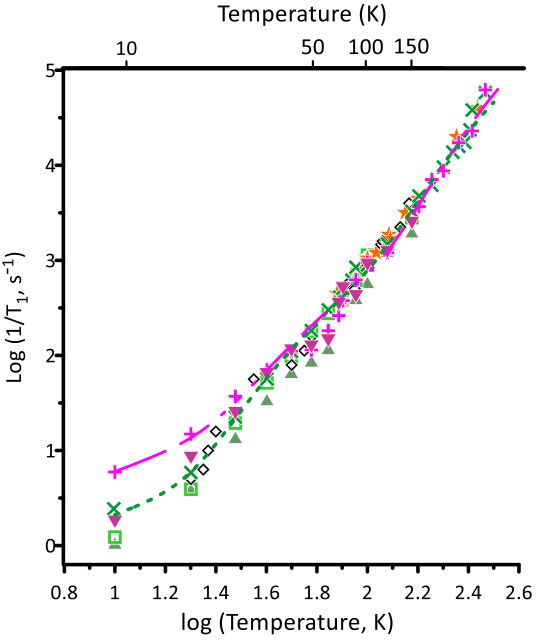

Fig. 3 Temperature dependence of T_1 obtained by inversion recovery for $^{13}C_1$-PTMTC in 9:1 trehalose:sucrose (pink+), $^{13}C_1$-dFT in 9:1 trehalose:sucrose (green x), $^{13}C_1$-PTMTC (pink inverted triangle), $^{13}C_1$-dFT (green triangle),$^{12}C_1$-dFT (green open square), and $^{12}C_1$-FT (olive x) in 1:1 PBS:glycerol; and by saturation recovery for $^{12}C_1$-dFT (orange star), and $^{12}C_1$-FT (black diamond) in 1:1 PBS:glycerol. Below about 30 K, the relaxation rates for $^{13}C_1$-PTMTC in 9:1 trehalose:sucrose are enhanced because of the high spin concentration. The lines are fits to $1/T_1$ for $^{13}C_1$-PTMTC (long dashes) or $^{13}C_1$-dFT (short dashes) in 9:1 trehalose:sucrose calculated as the sum of contributions from the direct, Raman, and local mode processes with the parameters discussed in the text

of the relaxation rates was modeled as the sum of direct, Raman [35, 36], and local mode [37, 38] processes as shown in Eqs. (5) and (6) [34].

$$\frac{1}{T_1} = A_{\mathrm{dir}}T + A_{\mathrm{Ram}}\left(\frac{T}{\theta_{\mathrm{D}}}\right)^9 J_8\left(\frac{\theta_D}{T}\right) + A_{\mathrm{loc}}\left[\frac{e^{\Delta_{\mathrm{loc}}/T}}{\left(e^{\Delta_{\mathrm{loc}}/T}-1\right)^2}\right], \tag{5}$$

where J_8 is the transport integral that is described by Eq. (6)

$$J_8\left(\frac{\theta_{\mathrm{D}}}{T}\right) = \int_0^{\theta_{\mathrm{D}}/T} x^8 \frac{e^x}{(e^x-1)^2}\mathrm{d}x, \tag{6}$$

and A_{dir} = coefficient of the direct process, A_{ram} = coefficient of the Raman process, θ_D = Debye temperature, A_{loc} = coefficient of the local mode, and Δ_{loc} = energy of the local mode. Below about 20 K, the process that depends linearly on T makes a significant contribution. The Raman process dominates between about 20 and 120 K and the contribution from the local mode is increasingly important at higher temperatures. It was possible to acquire data over a wider temperature range in 9:1 trehalose:sucrose, which facilitated a more accurate determination of the energy of the local mode than can be obtained in 1:1 PBS:glycerol. The fit lines for data in 9:1 trehalose:sucrose (Fig. 3) were obtained with $A_{dir} = 0.22\ s^{-1}$, $A_{Ram} = 1.4 \times 10^4\ s^{-1}$, $\theta_D = 160$ K, $A_{loc} = 4.9 \times 10^5\ s^{-1}$ and $\Delta_{loc} = 850$ K for $^{13}C_1$-dFT and with $A_{dir} = 0.6\ s^{-1}$, $A_{Ram} = 1.3 \times 10^4\ s^{-1}$, $\theta_D = 160$ K, $A_{loc} = 1.1 \times 10^6\ s^{-1}$ and $\Delta_{loc} = 1000$ K for $^{13}C_1$-PTMTC. The Debye temperature for the trehalose:sucrose matrix is higher than the value of 120 K observed in 1:1 water:glycerol [33]. The energy of the local mode for $^{13}C_1$-dFT is in good agreement with the value reported in 1:1 water:glycerol [34]. The energy for the local mode for $^{13}C_1$-PTMTC is slightly higher than for $^{13}C_1$-dFT.

Although there is scatter in the data in Fig. 3, the overall temperature dependence is similar for all of the samples, which leads to the conclusion that the chlorine substituents have little impact on T_1. Prior studies of the impact of chlorination on T_1 were complicated by differences in solubility that required use of different solvents for pairs of molecules with and without chlorine substituents. $1/T_1$ for PTM in 4:1 toluene:$CHCl_3$ was about 50% faster than for dFT in 1:1 water:glycerol between 25 and 250 K [17]. The hydrogen-bonded 1:1 water:glycerol glass is more rigid than 4:1 toluene:$CHCl_3$ which may have contributed to differences in the relaxation rates. Between about 125 and 250 K $1/T_1$ for 2,3,5,6-tetrachlorobenzosemiquinone in 2:1 triacetin:hexamethylphosphoramide was about a factor of 4 faster than for 2,5-dichloro-3,6-dihydroxy-1,4-benzosemiquinone in 1:1 water:glycerol. Here too, the relaxation rate for the more highly chlorinated molecule may have been increased by greater mobility in the non-hydrogen-bonded glass. In evaluating the trends for the semiquinones, it should be noted that the two additional chlorines resulted in an increase in g_{iso} of 0.0012; whereas, chlorination of $^{13}C_1$-PTMTC resulted in an increase of g_{iso} of only 0.0002 in 1:1 PBS:glycerol. Increasing g values, which are a surrogate for increasing spin orbit coupling, also contribute to faster spin–lattice relaxation.

4 Conclusions

^{13}C substitution at C_1 results in a highly anisotropic hyperfine coupling. Modulation of this anisotropic interaction provides an effective spin lattice relaxation mechanism in fluid solution. Chlorine substitution on the trityl rings has little additional impact on T_1 in fluid solution. In immobilized samples, $^{13}C_1$ substitution or chlorine substitution on the phenyl rings has negligible impact on T_1.

Acknowledgements Support of this work by NIH NCI R01 CA 177744 to GRE and SSE and NIBIB R00 EB023990 and R21 EB028553 to BD is gratefully acknowledged. Support from the University of Denver to GRE and SSE and from the WVU HSC startup funds for BD also are acknowledged.

References

1. B. Epel, M.K. Bowman, C. Mailer, H.J. Halpern, Magn. Reson. Med. **72**, 362–368 (2014)
2. B. Epel, H.J. Halpern, eMagRes **6**, 149–160 (2017)
3. N.-T. Chen, E.D. Barth, T.-H. Lee, B. Epel, H.J. Halpern, L.-W. Lo, Int. J. Nanomed. **14**, 2963–2971 (2019)
4. M.C. Krishna, S. Matsumoto, H. Yasui, K. Saito, N. Devasahayam, S. Subramanian, J.B. Mitchell, Radiat. Res. **177**, 376–386 (2012)
5. L. Lampp, O.Y. Rogozhnikova, D.V. Trukhin, V.M. Tormyshev, M.K. Bowman, N. Devasahayam, M.C. Krishna, K. Mader, P. Imming, Free Radic. Biol Med. **130**, 120–127 (2019)
6. K.-I. Matsumoto, F. Hyodo, J.B. Mitchell, M.C. Krishna, Magn. Reson. Med. **79**, 1212–1218 (2018)
7. B. Epel, H.J. Halpern, J. Magn. Reson. **254**, 56–61 (2015)
8. Z. Yang, Y. Liu, P. Borbat, J.L. Zweier, J.H. Freed, W.L. Hubbell, J. Am. Chem. Soc. **134**, 9950–9952 (2012)
9. Z. Yang, M.D. Bridges, C.J. Lopez, O.Y. Rogozhnikova, D.V. Trukhin, E.K. Brooks, V. Tormyshev, H.J. Halpern, W.L. Hubbell, J. Magn. Reson. **269**, 50–54 (2016)
10. G.Y. Shevelev, O.A. Krumkacheva, A.A. Lomzov, A.A. Kushelev, O.Y. Rogozhnikova, D.V. Trukhin, T.I. Troitskaya, V.M. Tormyshev, M.V. Fedin, D.V. Pyshnyi, E.G. Bagryanskaya, J. Am. Chem. Soc. **136**, 9874–9877 (2014)
11. G.Y. Shevelev, O.A. Krumkacheva, A.A. Lomzov, A.A. Kuzhelev, D.V. Trukhin, O.Y. Rogozhnikova, V.M. Tormyshev, D.V. Pyshnyi, M.V. Fedin, E.G. Bagryanskaya, J. Phys. Chem. B. **119**, 13641–13648 (2015)
12. O. Krumkacheva, E. Bagryanskaya, J. Magn. Reson. **280**, 117–126 (2017)
13. N. Fleck, C.A. Heubach, T. Hett, F.R. Haege, P.P. Bawol, H. Blatruschat, O. Schiemann, Angew. Chem. Int. Ed. **59**, 9767–9772 (2020)
14. M. Gomberg, J. Am. Chem. Soc. **22**, 757–771 (1900)
15. J.H. Ardenkjaer-Larsen, I. Laursen, I. Leunbach, G. Ehnholm, L.-G. Wistrand, J.S. Petersson, K. Golman, J. Magn. Reson. **133**, 1–12 (1998)
16. M. Ballester, J. Riera-Figueras, J. Castaner, C. Badfa, J.M. Monso, J. Am. Chem. Soc. **93**, 2215–2225 (1971)
17. V. Kathirvelu, G.R. Eaton, S.S. Eaton, Appl. Magn. Reson. **37**, 649–656 (2010)
18. W. Moore, J. McPeak, M. Poncelet, B. Driesschaert, S.S. Eaton, G.R. Eaton, J. Magn. Reson. **318**, 106797 (2020)
19. J.L. Huffman, M. Poncelet, W. Moore, S.S. Eaton, G.R. Eaton, B. Driesschaert, J. Phys. Chem. B **125**, 7380–7387 (2021)
20. M. Poncelet, B. Driesschaert, Angew. Chem. Int. Ed. **59**, 16451–16454 (2020)
21. S. Stoll, A. Schweiger, J. Magn. Reson. **178**, 42–55 (2006)
22. Y. Zhou, R. Mitri, G.R. Eaton, S.S. Eaton, Curr. Top. Biophys. **23**, 63–68 (1999)
23. N. Elewa, N. Maltar-Strmecki, M.M. Said, H.A. El Shihawy, M. El-Sadek, J. Frank, S. Drescher, M. Drescher, K. Mader, D. Hinderberger, P. Imming, Phys. Chem. Chem. Phys. **19**, 6688–6697 (2017)
24. J.C. Paniagua, V. Mugnaini, C. Gabellieri, M. Feliz, N. Roques, J. Veciana, M. Pons, Phys. Chem. Chem. Phys. **12**, 5824–5829 (2010)
25. P.W. Atkins, J. de Paula, *Physical Chemistry* (Freeman, New York, 2010), p. 769
26. D. Kivelson, P. Madden, Annu. Rev. Phys. Chem. **31**, 523–558 (1980)
27. R.E.D. McClung, D. Kivelson, J. Chem. Phys. **49**, 3380–3391 (1968)
28. R. Owenius, G.R. Eaton, S.S. Eaton, J. Magn. Reson. **172**, 168–175 (2005)
29. J.R. Biller, H. Elajaili, V. Meyer, G.M. Rosen, S.S. Eaton, G.R. Eaton, J. Magn. Reson. **236**, 47–56 (2013)
30. J.R. Biller, V. Meyer, H. Elajaili, G.M. Rosen, J.P.Y. Kao, S.S. Eaton, G.R. Eaton, J. Magn. Reson. **212**, 370–377 (2011)
31. S.S. Eaton, G.R. Eaton, Biol. Magn. Reson. **19**, 29–154 (2000)
32. T. Ngendahimana, R. Ayikpoe, J.A. Latham, G.R. Eaton, S.S. Eaton, J. Inorg. Biochem. (2019). https://doi.org/10.1016/j.jinorgbio.2019.110806
33. Y. Zhou, B.E. Bowler, G.R. Eaton, S.S. Eaton, J. Magn. Reson. **139**, 165–174 (1999)
34. A.J. Fielding, P.J. Carl, G.R. Eaton, S.S. Eaton, Appl. Magn. Reson. **28**, 231–238 (2005)
35. A. Abragam, *The Principles of Nuclear Magnetism* (Oxford University Press, Oxford, 1961)

36. J.W. Orton, *Electron Paramagnetic Resonance: An Introduction to Transition Group Ions in Crystals* (Gordon and Breach, New York, 1968)
37. J.G. Castle Jr., D.W. Feldman, J. Appl. Phys. **36**, 124–128 (1965)
38. J. Murphy, Phys. Rev. **145**, 241–247 (1966)
39. F.M. Vigier, D. Shimon, V. Mugnaini, J. Veciana, A. Feintuch, M. Pons, S. Vega, D. Goldfarb, Phys. Chem. Chem. Phys. **16**, 19218–19228 (2014)
40. A. Bos-Liedke, M. Walawender, A. Wozniak, D. Flak, J. Gapinski, S. Jurga, M. Kucinska, A. Plewinski, M. Murias, M. Elewa, L. Lampp, P. Imming, K. Tadyszak, Cell Biochem. Biophys. **76**, 19–28 (2018)
41. H.R. Falle, G.R. Luckhurst, A. Horsfield, M. Ballester, J. Chem. Phys. **50**, 258–264 (1969)